arXiv:1608.07181v1 [astro-ph.SR] 25 Aug 2016

Time resolved spectroscopy and photometry of three little known bright cataclysmic variables: LS IV -08° 3, HQ Monocerotis and ST Chamaeleontis[1]

Albert Bruch

Laboratório Nacional de Astrofísica, Rua Estados Unidos, 154, CEP 37504-364, Itajubá - MG, Brazil

Marcos P. Diaz

Instituto de Astronomia, Geofísica e Ciências Atmosféricas, Universidade de São Paulo, Rua do Matão, 1226, CEP 05508-090, São Paulo, Brazil

(Text published in: New Astronomy, Vol. 50, p. 109 – 119 (2017))

Abstract

As part of a project to better characterize comparatively bright but so far little studied cataclysmic variables in the southern hemisphere, we have obtained spectroscopic and photometric data of the nova-like variables LS IV -08° 3 and HQ Mon, and of the Z Cam type dwarf nova ST Cha. The spectra of all systems are as expected for their respective types. We derive improved orbital ephemeris of LS IV -08° 3 and map its accretion disk in the light of the Hα emission using Doppler tomography. We find that the emission has a two component origin, arising in the outer parts of the accretion disk and possibly on the illuminated face of the secondary star. The light curve of LS IV -08° 3 exhibits a low level of flickering and indications for a modulation on the orbital period. Spectroscopy of HQ Mon suggests an orbital period of $\approx 5^{\rm h}.15$ which is incompatible with previous (uncertain) estimates. The light curves show the typical low scale flickering of UX UMa type nova-like systems, superposed upon variations on longer time scales. During one night a modulation with a period of $\approx 41^{\rm m}$ is observed, visible for at least 4 hours. However, it does not repeat itself in other nights. A spectroscopic orbital period of $\approx 5^{\rm h}.5$ is derived for ST Cha. A previously suspected period of $6^{\rm h}.8$ (or alternatively $9^{\rm h}.6$), based on historical photographic photometry is incompatible with the spectroscopic period. Moreover, we show that our new as well as previous photometry does not contain evidence for the quoted photometric period.

Keywords: Stars: novae, cataclysmic variables – Stars: individual: LS IV -08° 3 – Stars: individual: HQ Mon – Stars: individual: ST Cha

[1]Based on observations taken at the Observatório do Pico dos Dias / LNA

1 Introduction

Cataclysmic variables (CVs) are interactive binaries where a late type, low mass star which is normally on or close to the main sequence transfers matter to a white dwarf. For a general and encompassing introduction to CVs, see Warner (1995) or Hellier (2001). The number of known systems of this kind has grown enormously in recent years mainly due to numerous detections of CVs in large scale surveys. However, most of these newly discovered systems are rather faint in their normal brightness state. Therefore, the characterization of their individual properties is expensive because is requires large telescopes.

On the other hand, it is much easier to perform detailed studies of the brighter CVs, most of which are known for a long time. It is therefore surprising that even among these stars an appreciable number has not yet been adequately characterized to be certain about basic parameters such as the orbital period. In some cases even the very class membership is not confirmed.

We therefore started a small observing program aimed at a better understanding of these so far neglected stars. For this purpose we selected a number of little studied southern CVs and suspected CVs bright enough ($m_{\rm vis} \leq 15^{\rm m}$) to be easily observed with comparatively small telescopes. The emphasis of this program lies on photometry with a high time resolution aimed at the detection of short and medium time scale variations such as flickering and orbital variability. However, in a few cases the photometric observations could be complemented by spectroscopic time series. The first results of this program, concerning the dwarf nova MU Cen, were recently published by Bruch (2016).

Here, we report on three stars for which spectra were taken in addition to light curves. These are the nova-like variables LS IV -08$^{\rm o}$ 3 and HQ Mon, and the Z Cam type dwarf nova ST Cha. Nova-like variables are CVs with accretions disks in a bright state which do not show outbursts such as the dwarf novae (or, alternatively, may be considered to be in permanent outburst). Sometimes, they are subdivided into UX UMa stars which always remain on approximately the same brightness level, and VY Scl stars which occasionally assume a low state at much fainter magnitude than normal. The Z Cam stars are systems which, instead of alternating between quiescent and outburst states due to a limit cycle instability in their accretion disks as is usual with dwarf novae, sometimes get stuck for some time at a brightness just below the outburst level. This phenomenon in known as "standstill".

HQ Mon and ST Cha entered the observing program mainly because no time resolved photometry was ever published and because the orbital periods as quoted in the most recent on-line edition of the Ritter & Kolb catalogue (Ritter & Kolb 2003) are uncertain and require confirmation. On the other hand, LS IV -08$^{\rm o}$ 3 was quite thoroughly characterized by Stark et al. (2008). It entered the observing program only as a backup target. However, as it turns out, the present additional observations nicely complement those of Stark et al. (2008).

In Sect. 2 we report briefly on the observations and data reductions. The results for the indivivual objects are then dealt with in turn in Sects. 3 – 5. We summarize the most important conclusions in Sect. 6.

2 Observations and data reductions

All observations were obtained at the Observatório do Pico dos Dias (OPD), operated by the Laboratório Nacional de Astrofísica, Brazil. For photometry the 0.6-m Zeiss and the 0.6-m Boller & Chivens telescopes were used. Spectroscopy was performed using the 1.6-m Perkin Elmer telescope.

Table 1: Journal of photometric observations

Name	Date	Start (UT)	End (UT)	Time Res. (s)	Number of Integr.
LS IV -08^{o} 3	2015 May 20	1:10	6:16	6	3 449
	2015 May 21	3:35	6:52	6	1 971
HQ Mon	2014 Mar 26	23:19	23:52	5.5	346
	2014 Mar 28/29	23:05	1:52	5.5	2 094
	2014 Nov 21	3:20	7:34	5	2 923
	2015 Feb 13	0:59	5:02	5	2 645
ST Cha	2014 Mar 29	2:52	5:22	5.5	1 466
	2014 Apr 30	21:38	22:00	5	256
	2014 Jun 17/18	21:25	0:18	5	1 800

Time series imaging of the field around the target stars was performed using cameras of type Andor iXon EMCCD DU-888E-C00-#BV and iKon-L936-B equipped with back illuminated, visually optimized CCDs. In order to resolve the expected rapid flickering variations the integration times were kept short. Together with the small readout times of the detectors this resulted in a time resolution of the order of 5^{s}. In order to maximize the count rates in these short time intervals no filters were used. Therefore, it was not possible to calibrate the stellar magnitudes. Instead, the brightness was expressed as the magnitude difference between the target and a nearby comparison star. This is not a severe limitation in view of the purpose to the observations. A summary of the photometric observations is given in Table 1. Not all of them were useful. Parts with an elevated noise level due to passing clouds will not be regarded here.

The spectra were taken in 2015, February and March, using the Boller & Chivens spectrograph of OPD. Details are given in Table 2. An Andor iKon-L936-BR-DD camera was employed. Integration times were 15^{m} throughout. Exposures of a He-Ar lamp for wavelength calibration were taken after every second stellar exposure. From the FWHM of the lines in the comparison spectra a spectral resolution of $\approx$4 Å is estimated. The spectral range of the March data encompassed Hα and Hβ. However, due to a error of the instrumental configuration, Hα was not included in the February spectra. The observing conditions were quite variable, ranging from photometric to periods heavily affected by clouds. Therefore, some of the spectra remained severely underexposed and are only of limited usefulness. In view of these difficulties no attempt was made to flux calibrate the data.

Basic reductions of the data (bias subtraction, flat-fielding, spectral extraction) were performed with IRFF. All further data reduction and analysis was done using the MIRA software system (Bruch 1993), with the exception of the Doppler mapping (Sect. 3.1) for which an IRAF/SPP user code was employed.

Aperture photometry was applied to the images of the target stars, the primary comparison stars and several check stars in the field. The time axis of the resulting light curves is expressed in UT throughout this paper, unless stated otherwise. In contrast, the times of mid-exposure of the spectra, used to measure the orbital motion of the target stars, were transformed into barycentric Julian Dates, following Eastman et al. (2010). In order to remove the instrumental response curve from the uncalibrated spectra, they were normalized to the continuum. The raw spectra contained strong absorption features in particular in the

Table 2: Journal of spectroscopic observations

Name	Date	Start (UT)	End (UT)	Number of Spectra	Spectral Coverage (Å)
LS IV -08^{o} 3	2015 Mar 24	5:33	8:35	11	4704 – 6796
	2015 Mar 25	4:35	8:21	12	4705 – 6797
	2015 Mar 26	4:24	6:00	6	4706 – 6798
	2015 Mar 27	4:06	8:27	16	4707 – 6799
	2015 Mar 28	4:34	7:31	9	4709 – 6801
HQ Mon	2015 Fev 13	0:57	4:46	12	4342 – 6448
	2015 Fev 14	2:48	4:31	6	4343 – 6449
	2015 Mar 24	21:51	22:07	1	4708 – 6800
	2015 Mar 25	21:39	22:50	2	4709 – 6801
	2015 Mar 26/27	21:37	1:56	15	4708 – 6800
ST Cha	2015 Fev 13	4:54	7:11	4	4339 – 6445
	2015 Mar 23/24	23:54	5:22	14	4702 – 6794
	2015 Mar 24/25	22:40	3:30	16	4702 – 6794
	2015 Mar 25/26	22:58	4:14	18	4704 – 6798
	2015 Mar 27	2:01	3:56	6	4707 – 6799

wavelength ranges $\lambda\lambda$ 5860 – 6020 Å (mostly just to the red of the Na D lines), $\lambda\lambda$ 6260 – 6340 Å and $\lambda\lambda$ 6450 – 6620 Å (to the blue and around Hα). They can be attributed to atmospheric absorptions. Therefore, the normalized spectra were divided by a suitably scaled normalized atmospheric transmission spectrum (degraded to match the observed spectral resolution). This procedure was optimized for the strong absorptions close to Na D and around Hα, at the expense of an imperfect elimination of the absorptions in the third range, resulted in spurious structures centred on $\lambda \sim$6280 Å in LS IV -08^{o} 3 and HQ Mon. With few exceptions which will be appropriately specified below radial velocities of lines in individual spectra were measured relative to the corresponding lines in the average spectrum by means of cross correlation: the maximum of a Gaussian fit to the cross-correlation function was used to calculate the radial velocity difference between the average and the individual spectra. Throughout this paper we define as spectroscopic phase zero the negative-to-positive zero-crossing of the Hα emission line radial velocity curve. In the ideal case (radially symmetric emission distribution confined to the accretion disk) this corresponds to the upper conjunction of the secondary star with respect to the white dwarf.

3 LS IV -08^{o} 3

We will start the discussion of the results with the best known of the three target stars, LS IV -08^{o} 3. At $V \approx 11\overset{m}{.}5$ (Høg et al. 2000) it is also the brightest. LS IV -08^{o} 3 was originally classified as an OB star (Nassau & Stephensen, 1963). Stark et al. (2008) narrate more of the history of our knowledge about this object. They performed a detailed spectroscopic study and found that LS IV -08^{o} 3 is a binary with a period of 0.1952894 days. The characteristics of the system suggested a reclassification as a nova-like variable of the UX UMa subtype. Stark et al. (2008) also present some time resolved photometry which reveals low scale (a few hundredths of a magnitude) apparently stochastic variations

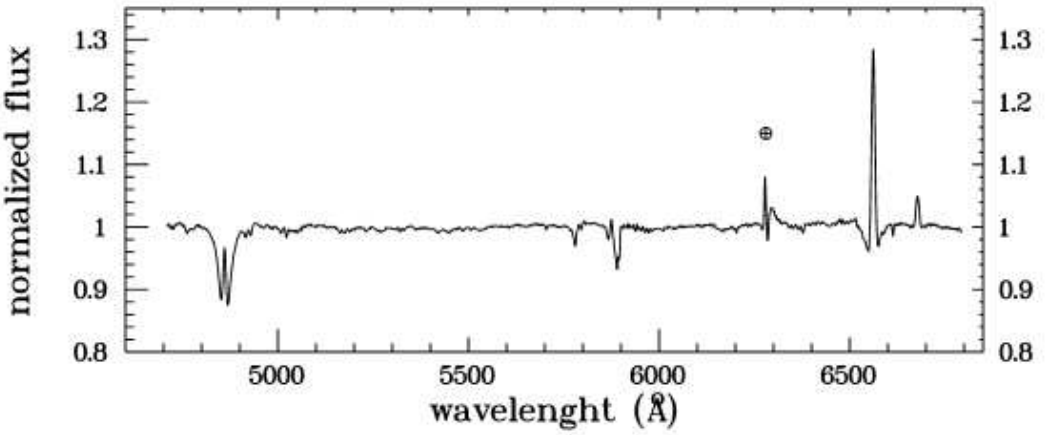

Figure 1: Average continuum normalized spectrum of LS IV -08^{o} 3. (The marked structure is an artifact caused by an imperfect removal of atmospheric absorption features.)

superposed on slight orbital variations.

3.1 Spectroscopy

Spectra of LS IV -08^{o} 3 were obtained in five nights in 2015, March. The average spectrum, weighting the individual spectra by their mean count rates, is shown in Fig. 1. The marked structure around $\lambda \sim$6280 Å resulted from an imperfect elimination of atmospheric absorption lines (see Sect. 2).

The spectrum resembles very much that shown in Fig. 2 of Stark et al. (2008) and which is quite typical for CVs with accretion disks in the bright state: Balmer emission components decreasing in strength from Hα to Hβ are superposed upon broad absorption troughs which are stronger for the higher Balmer lines. It appears that the centre of the Hα absorption is somewhat shifted to the blue with respect to the emission component. This is not the case for Hβ. He I $\lambda\lambda$ 5876 Å and 6678 Å are also seen in emission[2]. The Na D absorption at $\lambda\lambda$ 5890-5896 Å is not expected in the spectrum of a nova-like variable and is interpreted as interstellar by Stark et al. (2008). This is confirmed here (see below). Finally, the absorption feature at λ 5780 Å is a diffuse interstellar band. Not surprisingly, we measure its equivalent width to be identical to that measured by Stark et al. (2008).

The strength of the Hα emission line and the good S/N-ratio of the spectra permitted to apply the double Gaussian convolution method proposed by Schneider & Young (1980) to measure the line position. The separation a of the two Gaussians was chosen to be between 1 Å and 7 Å, fixing their width to 1 Å. We then used the diagnostic diagrams first introduced by Shafter (1983) and later refined by Shafter et al. (1986) in order to determine the optimal orbital solution. The period was fixed to the value found by Stark et al. (2008).

It was found that the dependence of the orbital solution on a is quite weak. Within the sampled range of a, the amplitude of the radial velocity (RV) variations did not vary by more than 6 km/sec, the γ-velocity remained stable within 7 km/sec, and the phase shift was limited to 0.012. Thus, there is no strong indication that different parts of the line profile follow distinct radial velocity curves (but see the results of Doppler mapping of Hα

[2]The impression that He I λ 5876 Å is superposed on the blue flank of the broad Na D absorption may have been enhanced by uncertainties in the continuum normalization in this range.

that will be presented below). In order to be definite, and following the criterium normally used in the interpretation of the diagnostic diagrams, we choose the solution for $a = 5.2$ Å as reference. This is the values at which the relative error σ_K/K of the RV amplitude assumes a (shallow) minimum. The corresponding RV curve, after applying the heliocentric correction, is shown in the lower frame of Fig. 2 together with the best fit sine curve.

The sine fit resulted in an amplitude of the RV curve of $K = 82 \pm 4$ km/sec. This is slightly higher than the values measured by Stark et al. (2008) (77 ± 4) but still compatible within the error limits. However, the presently found γ velocity (-21 ± 3 km/sec) is rather different from their value (-44 ± 3 km/sec).

The weaker Hβ emission did not warrant the application of the double Gaussian convolution method in order to determine the line position. Therefore, the cross correlation method was applied in three different ways: (i) using the entire line profile (absorption and emission component), (ii) masking the emission component and cross-correlating only the absorption component, and (iii) cross-correlating only the emission component, after dividing the entire line profile by a high order polynomial fit to the absorption component (emission masked). The resulting radial velocity values were very similar. In the central frame of Fig. 2 the RV curve, folded on the orbital period, of the emission component is shown together with the best fit sine curve. At $K = 83 \pm 7$ km/sec, the amplitude is almost identical to the one measured for Hα. This is another indication that their are no strong differences in the contribution to the hydrogen emission lines from different parts of the binary system. Due to the cross-correlation method applied here, the velocity zero-point of Hβ is, of course, arbitrary.

The orbital period $P_{\rm orb}$ of LS IV -08$^{\rm o}$ 3 derived by Stark et al. (2008) is based on spectra taken between 2004 and 2007. The present new data enlarge the total time base and thus enable a refinement of the period. The accuracy of the value quoted by Stark et al. (2008) is high enough to preserve cycle counts up to the present epoch. They used the same phase convention as we did (see their Fig. 3). However, adopting their ephemeris, we observe a phase difference of 0.17 ± 0.09 (Hα) and 0.18 ± 0.09 (Hβ) with respect to the radial velocities of 2015, March. Assigning (arbitrarily) twice as much weight to the phase difference of Hα than to that of Hβ, and attributing it to a slight period error, results in refined ephemeris:

$$\mathrm{BJD} = 2457107.7527(19) + 0.1952913(3) \times E$$

where E is the cycle number. The epoch is close to the mean epoch of the present observations. The errors are given in units of the last decimal digits. For the epoch, it corresponds simply to the phase difference found between the best sine fit to the Hα and Hβ RV curves. The error of the period is estimated from the error quoted by Stark et al. (2008), assuming that it scales inversely with the total time base of the observations.

The He I λ 6678 Å emission line behaves slightly different from the Balmer lines. Measuring the line position via cross-correlation with the mean line profile yields the radial velocity curve, folded on $P_{\rm orb}$ using the above ephemeris, shown in upper frame of Fig. 2. With 112 ± 6 km/sec the best fit sine curve has an amplitude which is significantly larger than that of the Balmer lines. Such differences in the RV amplitudes of different lines are not uncommon in cataclysmic variables (see, e.g., the dramatic difference of the RV amplitude of Hβ and He II λ 4686 Å in HR Del; Bruch 1982) and can complicate a lot dynamical interpretations of line motions. Moreover, there is a definite phase shift of -0.05 between the He line and the Balmer lines. Both findings point at differences in the emission sites of helium and hydrogen. We refrain from trying to measure the radial velocity of He I λ 5876 Å because of its superposition upon the blue flank of the Na D absorption.

Finally, for the sake of exercise, we also cross-correlated the Na I D lines of the individual spectra with their average, carefully avoiding the He I λ 5786 Å emission line located on the

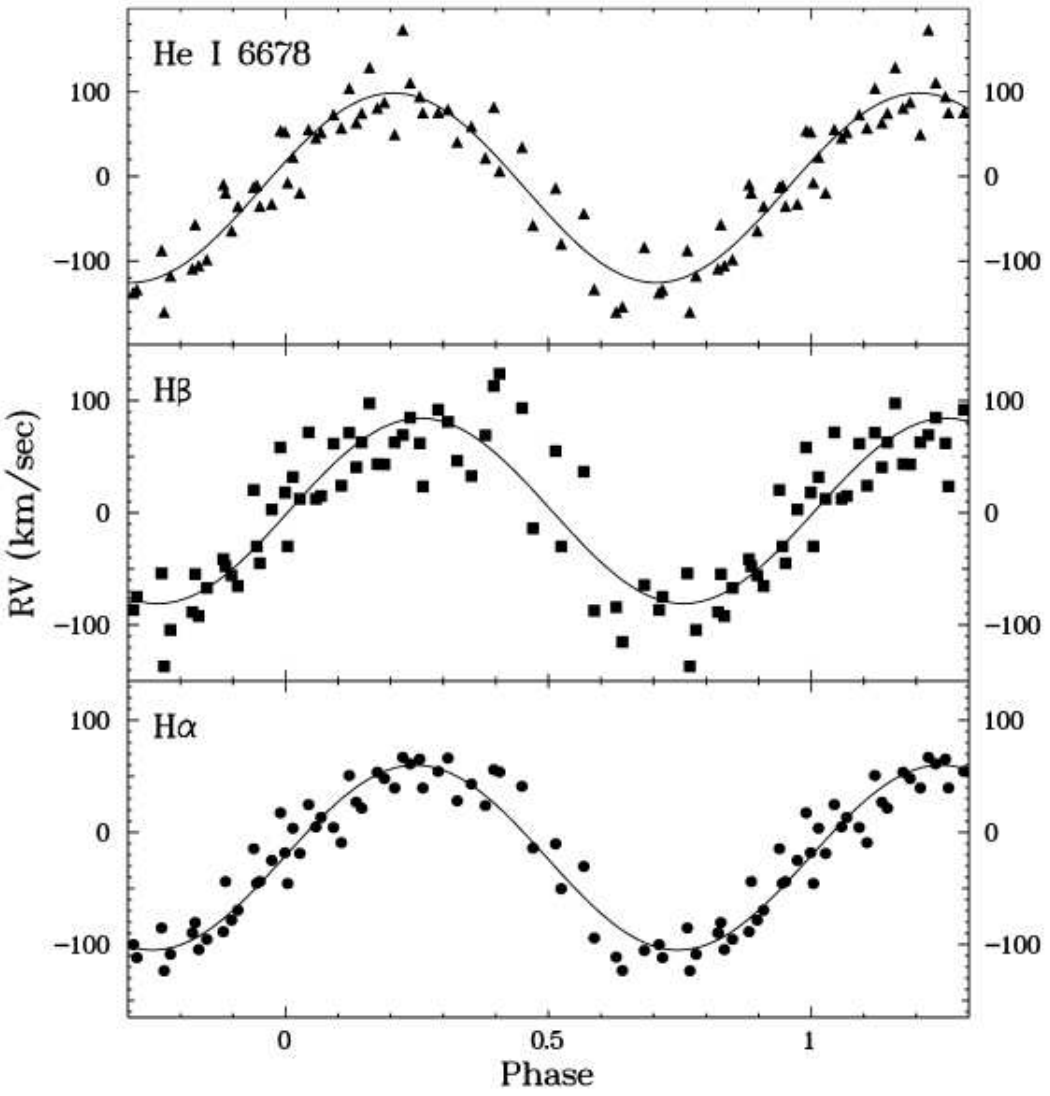

Figure 2: Radial velocity curve of the He I λ 6678 Å (top), Hβ (centre) and Hα (bottom) emission lines of LS IV -08^{o} 3. The zero points of the He I and Hβ curves are arbitrary, while for Hα heliocentric velocities are plotted.

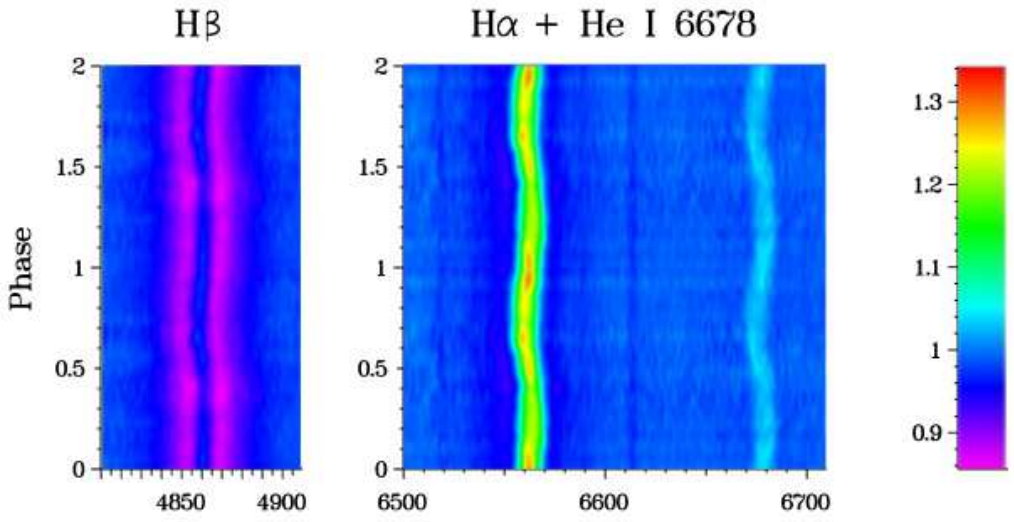

Figure 3: Spectra of Hβ and Hα + He I λ 6678 Å as a function of orbital phase. The scale of the colour bar at the right is given in units of the continuum intensity.

blue flanc of the absorption feature. As expected, no radial velocity variations were found, confirming the identification by Stark et al. (2008) of these lines as interstellar.

Fig. 3 shows the trailed spectra of Hβ and Hα + He I λ 6678 Å as a function of phase. The radial velocity variations of all lines are readily visible. As mentioned earlier, the Hα emission is not centralized within the shallow absorption trough (see the asymmetry of the dark blue shade on both sides of the emission in the figure). In their high-resolution HET spectra of LS IV -08$^{\rm o}$ 3 Stark et al. (2008) detected changes in the shape of the Hα emission profile which they consider to be composed of a broad and a narrow component moving in anti-phase. They tentatively identify the former as arising from the accretion disk and the latter from the side of the mass donating star facing and being illuminated by the primary component of the CV.

At the much lower resolution of the present data these details cannot be seen directly. However, a close inspection of Fig. 3 shows that the normalized strength of the emission components of both, Hα and Hβ, exhibits variations as a function of phase. This is also seen in Fig. 4 where in the lower frames the equivalent width of the emission (expressed as positive values for simplicity) is plotted as a function of phase. In spite of considerable noise, a clear phase dependence is visible in both lines. We also measured the line width (upper frames of Fig. 4, expressed as the FWHM of a Gaussian fitted to the emission. While no systematics can be seen in the case of Hβ, the Hα line width exhibits a strikingly clear modulation on half the orbital period, assuming minima at phase 0 and 0.5.

In order to verify if this modulation can be explained by structures in the accretion disk, a Doppler map of the Hα emission was calculated using an algorithm known as filtered back projection. The mathematics related to this method are described in detail by Rosenfeld & Kak (1982). Before processing the data, the continuum around Hα and the average absorption profile, approximated (and interpolated beneath the emission) by a high order polynomial, were subtracted from the individual spectra. The orientation of the Doppler map depends on the orbital phase. Having no independent reliable information (e.g., through eclipse measurements), we trust that the spectroscopic zero point of the phase given by the

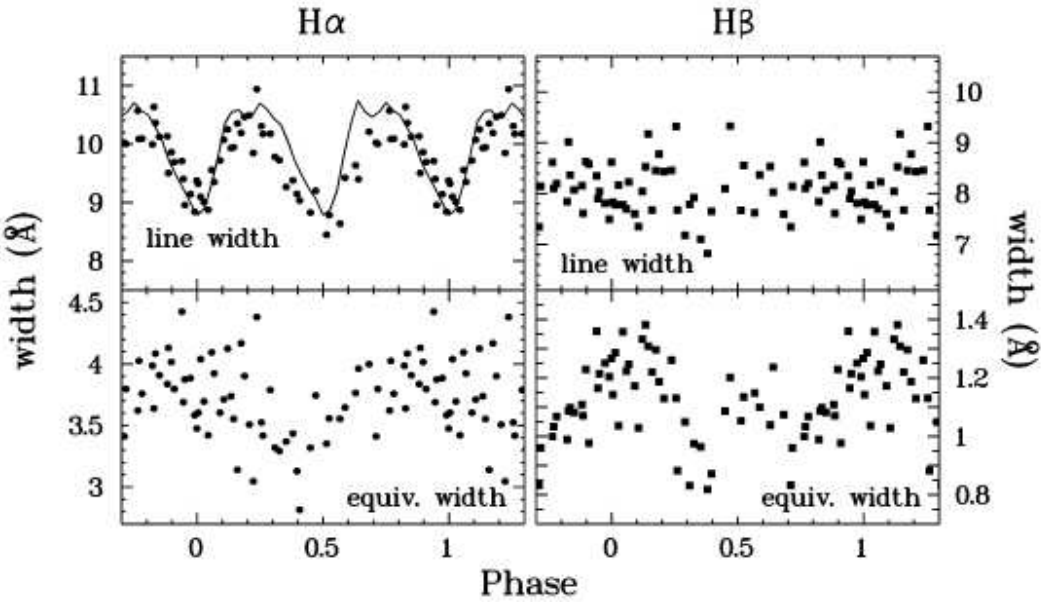

Figure 4: Line width (FWHM of a Gaussian fitted to the line) and equivalent width of the emission components of Hα and Hβ as a function of phase. The solid line in the upper left frame represents the line width reconstructed from the Doppler map (see text).

orbital ephemeris refers to the upper conjunction of the secondary star.

The resulting Doppler map is shown in Fig. 5. Only for illustrative purposes we include in the map as a yellow line the Roche lobe contours of the binary, assuming – in the absence of any more detailed information about the respective parameters – arbitrarily an orbital inclination of 60$^{\rm o}$, a primary star mass of 0.83 $M_{\odot}$, i.e. the mean mass of the white dwarf in CVs according to Zorotovic et al. (2011), and a secondary star mass of 0.43 $M_{\odot}$, based on the semi-empirical relation between the mass of the secondary stars in CVs and their orbital period derived by Knigge et al. (2011). Thus, the assumed mass ratio is $q = M_2/M_1 = 0.52$. The blue line is then the trajectory of the mass transfer stream from the secondary to the accretion disk. The resolution (FWHM) of the map is ∼200 km/s, corresponding to 4.4 Å, comparable to the spectral resolution quoted in Sect. 2.

The limited resolution of the Doppler map does not permit to identify many details. At high velocities the map shows symmetric emission around the white dwarf, resembling the Doppler maps of bright steady state disks with single peaked emission components (e.g., the SW Sex type system V347 Pup; Diaz & Hubeny 1999). There is no indication of a hot spot which, if present, should be placed at elevated velocities on the stream trajectory (blue line). Most of the emission is confined to low velocities, representing the outer regions of the accretion disk. The emission structure is somewhat elongated along the line connecting the stellar components of LS IV -08$^{\rm o}$ 3. On close inspection, two separated nuclei can be distinguished, one of them centred on the primary star. The other one is shifted into the direction of the secondary star. It would be close to the inner Lagrangian point if $q \gtrsim 0.6$ is chosen. Considering the standard deviation of CV white dwarf masses around their average (0.23 $M_{\odot}$, Zorotovic et al. 2011) such a mass ratio can, of course, easily be realized. Moreover, in combination with the assumed secondary star mass it does not violate stability criteria derived from recent binary population synthesis models (Schreiber et al. 2016). The

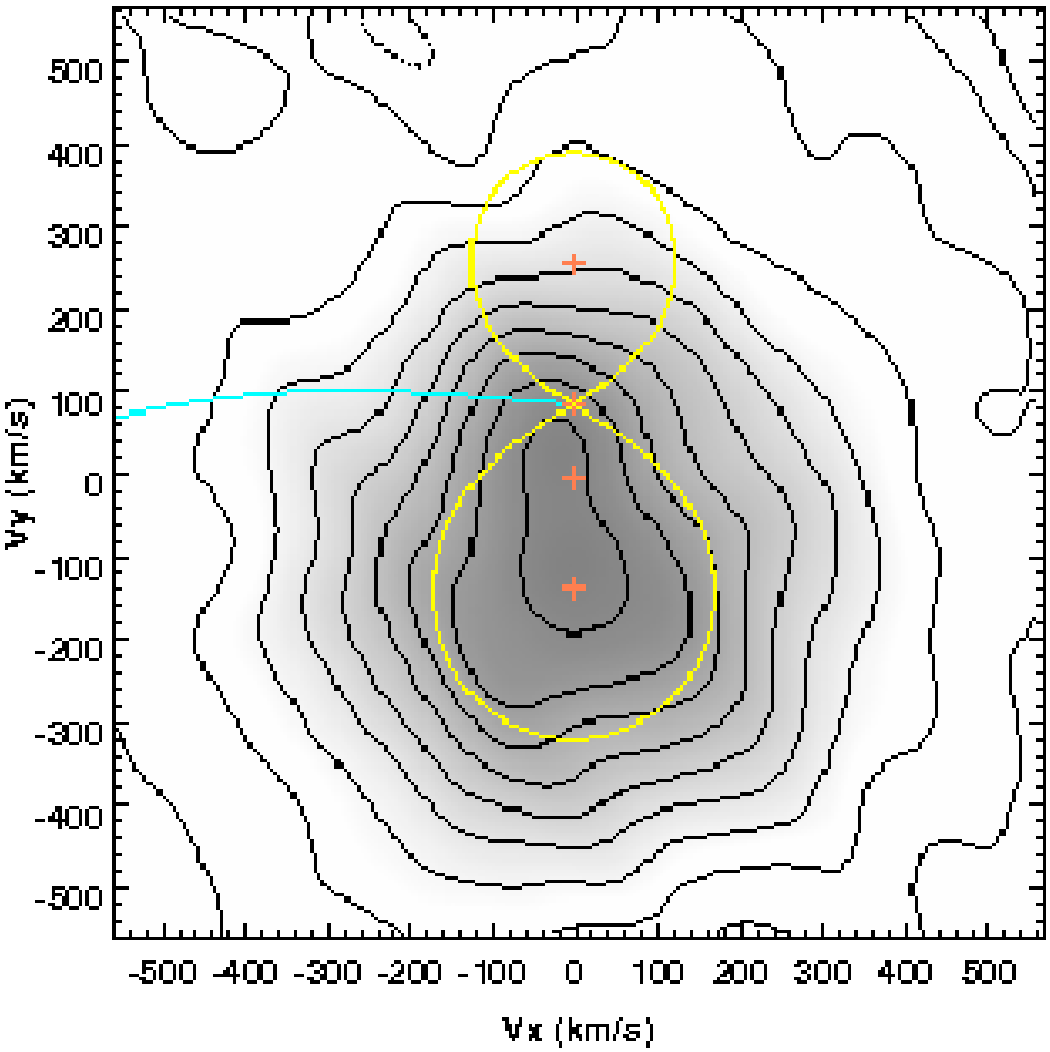

Figure 5: Doppler map of the Hα emission line of LS IV -08^{o} 3, expressed on a linear flux scale. The yellow contours indicate the location of the Roche lobe, assuming (arbitrarily) an orbital inclination of 60^{o}, and masses of 0.75 $M_{\odot}$ and 0.43 $M_{\odot}$, respectively, for the primary and secondary components of system. The blue line then indicates the expected stream trajectory from the mass donor star.

origin of this emission may therefore be on the illuminated surface of the secondary star. This is then compatible with the interpretation of the narrow emission component identified by Stark et al. (2008) as arising on the mass donor.

The elongated structure is responsible for the modulation of the width of the Hα emission seen in Fig. 4. Whenever the line of sight is aligned with the line connecting the two nuclei their movement is perpendicular to the line of sight and the velocity dispersion attains a minimum. A quarter of an orbit later the nuclei move along the line of sight to the observer and thus the velocity dispersion is maximal. This can also be seen when reconstructing the emission line from the Doppler map. For this purpose the map was collapsed in the direction of the line of sight as a function of the orbital phase. The FWHM of a Gaussian fit to the resulting distribution is superposed upon the directly measured line width as a solid line in the upper left frame of Fig. 4. It shows a similar modulation as the directly observed line width.

3.2 Photometry

Light curves of LS IV -08$^{\rm o}$ 3 were observed in two consecutive nights (2015, May 20 and 21). They are shown in Figs. 6. Differential magnitudes are given with respect to the comparison star TYC 5642-0042-1 ($V_T = 11\overset{\rm m}{.}18$; $B_T = 12\overset{\rm m}{.}39$). This is the same star used by Stark et al. (2008) for their photometry of LS IV -08$^{\rm o}$ 3. Both light curves are characterized by gradual variations on hourly time scales, superposed by irregular flickering activity with a typical amplitude of the order of $0\overset{\rm m}{.}06$ (average of the two light curves, ignoring variations on time scales longer than $\approx 1^{\rm h}$ and occasional stronger flares. This compares well with the flickering amplitudes of other UX UMa type novalike variables. Using results of Beckemper (1995) we calculate these to be typically $0\overset{\rm m}{.}05$ (median of 63 light curves of 7 objects). The corresponding numbers for other CV types are (with increasing median amplitude): dwarf novae in outburst (rise, maximum or decline; excluding supermaxima ocurring in short period dwarf novae of SU UMa type): $0\overset{\rm m}{.}07$ (122 light curves of 28 objects); classical novae in quiescence: $0\overset{\rm m}{.}10$ (80 light curves of 10 objects); VY Scl stars in their high state: $0\overset{\rm m}{.}18$ (34 light curves of 5 objects) and dwarf novae in quiescence: $0\overset{\rm m}{.}29$ (79 light curves of 15 objects)[3].

Although the data consist only of two light curves the finding of Stark et al. (2008) of low amplitude orbital modulations of the brightness of LS IV -08$^{\rm o}$ 3 can be substantiated by the present observations. To show this, first the average nightly magnitude was subtracted from the light curves in order to eliminate possible night-to-night variations common in CVs and also seen in LS IV -08$^{\rm o}$ 3 (see Fig. 6 of Stark et al. 2008). They were then binned into intervals of $0.01P_{\rm orb}$ and time was transformed into barycentric Julian Date. Folding the resulting data on $P_{\rm orb}$ then results in the light curve shown in Fig. 7 where data from different nights are distinguished by different symbols.

The phase folded light curve exhibits a sinusoidal modulation with a total amplitude of $\approx 0\overset{\rm m}{.}04$. Some deviating points can be explained as being caused by particular flickering spikes. The brightness assumes a maximum close to spectroscopic phase 0.36 and a minimum near phase 0.86. While the current observations thus confirm the presence of orbital variations, their phasing is just the opposite of that found by Stark et al. (2008) (see the lower frame of their Fig. 6).

[3]These numbers should only be regarded as rough indications. A systematic study on this and other statistical properties of the flickering in many CVs is being prepared by the first author.

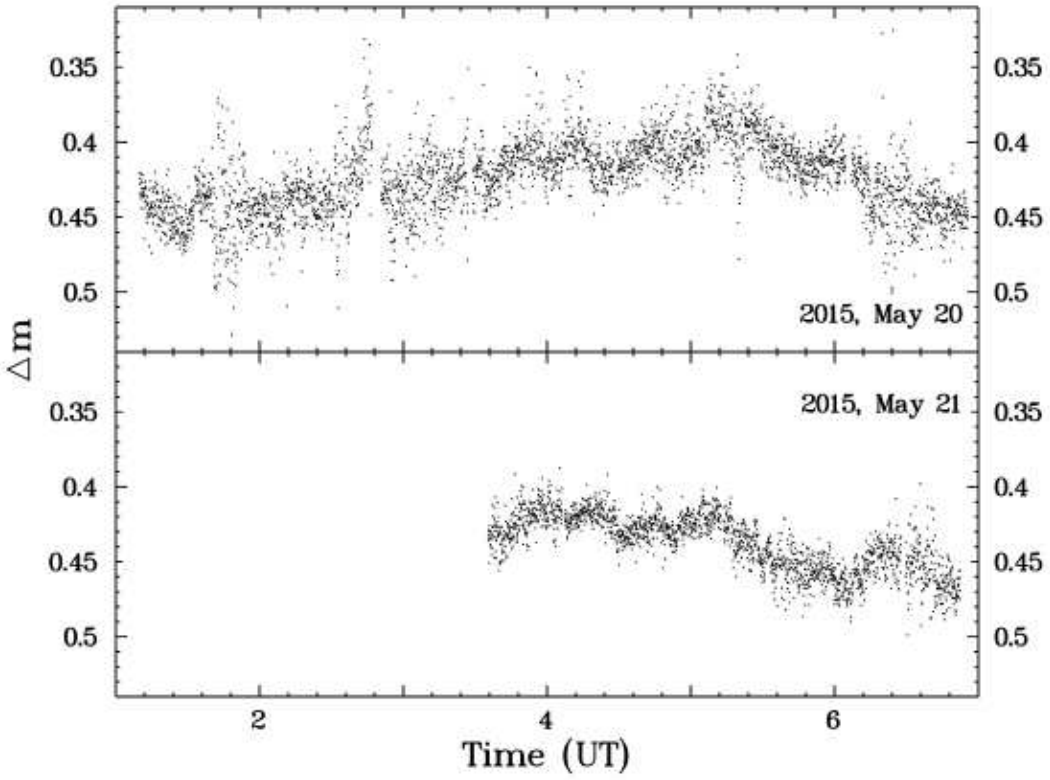

Figure 6: Differential light curves of LS IV -08° 3 in two nights in 2015, May.

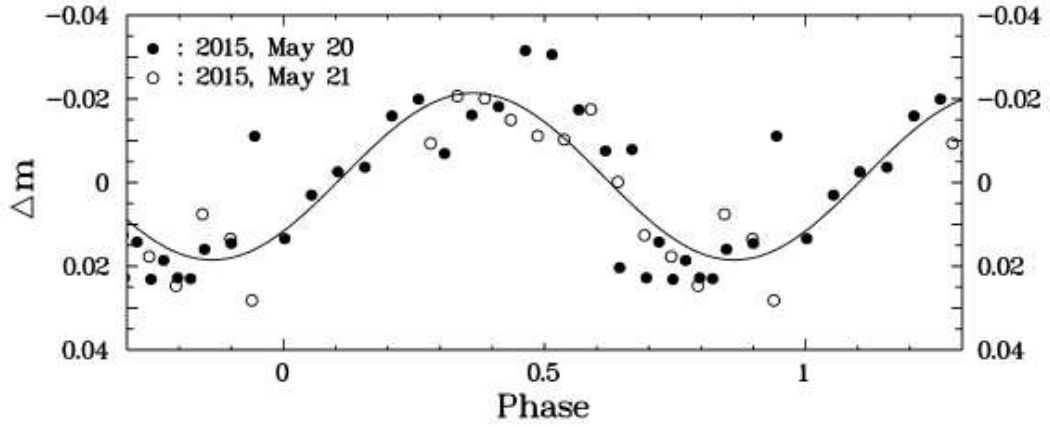

Figure 7: Light curves of LS IV -08° 3 folded on the spectroscopic period. Data from different nights are distinguished by different symbols.

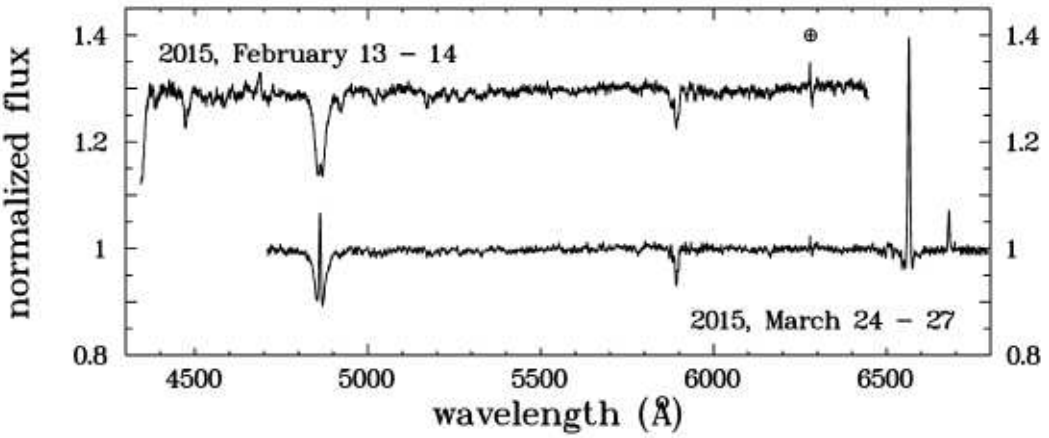

Figure 8: Average continuum-normalized spectra of HQ Mon in 2015, February and March. The February spectrum has been shifted upward by 0.3 units for clarity. (The marked structure is an artifact caused by an imperfect removal of atmospheric absorption features.)

4 HQ Monocerotis

HQ Mon is classified as RV: (RV Tau star with questionable classification) in the on-line version of the General Catalogue of Variables Stars (Samus et al. 1975), i.e. a radially pulsating supergiant. It was discovered by Morgenroth (1933) who describes its variations as "slowly variable" with a range between $13\overset{m}{.}5$ and $14\overset{m}{.}5$. The RV Tau classification first appears in the study of van Bueren (1950). Lloyd Evans (1984) found the spectrum to contain shallow hydrogen lines, and says that the UBV colours "confirm that it is a B star" According to the tables of Schmidt-Kaler (1982) this is true for the measured mean $U - B = -0.77$ but not for his $B - V = 0.04$ which is too red. Instead, the colours are compatible with those of a cataclysmic variable (Bruch & Engel 1994).

Van Bueren's (1950) classification of HQ Mon is questioned by Wahlgren et al. (1985) who describe the spectrum as containing hydrogen emission components within broad absorption lines together with emission of He II λ 4686. Wahlgren (1992) notes that the star resembles a cataclysmic variable "with a period of 32 days" (which is evidently not meant to be the orbital period). A low resolution spectum is reproduced by Zwitter & Munari (1994). It has a continuum rising steeply to short wavelengths. Hα and He II λ4686 are in emission, but only a broad absorption is seen at Hβ. The Na D absorption lines are also discernible. The orbital period of $7\overset{h}{.}59$ quoted in the Ritter & Kolb catalogue is based on an informal communication by J. Patterson [4] and requires confirmation.

4.1 Spectroscopy

Spectra of HQ Mon were obtained in two nights in 2015, February and in three nights in 2015, March (see Table 2). The average spectrum, weighing the individual spectra by their mean count rates, for the February and March observing runs are shown in Fig. 8 (for clarity the February spectrum was shifted upwards by 0.3 units).

The March spectrum resembles very much that of LS IV -08^o 3 but the Hβ emission component and (less so) the He I λ 6678 Å line are stronger. Again, the Na D lines are

[4] http://cbastro.org/communications/news/messages/0301.html

probably interstellar. The spectrum reproduced by Zwitter & Munari (1994) differs somewhat from the March spectrum in the sense that the emission component of Hβ is absent. But in this respect it is similar to the present February spectrum, where only a faint emission core appears at the bottom of the broad Hβ absorption line. Thus, significant variations of the hydrogen emission line strength in HQ Mon occur. Unfortunately, Hα was not covered in February, but in compensation the respective spectrum confirms the presence of He II λ 4686 Å in emission.

The absorption line at $\lambda \sim$4473 Å was also seen by Wahlgren et al. (1985) who attribute it to He I λ 4471 Å and Mg II λ 4481 Å. They contemplate a classification of HQ Mon as a Be star, in line with the presence of this absorption, but reject this idea because emission of He II λ 4686 Å would not be expected in a Be star. He I λ 4471 Å is seen in emission in numerous cataclysmic variables (most often in dwarf novae in quiescent) but relevant compilations of CV spectra (Bruch, 1989; Bruch & Schimpke, 1992; Zwitter & Munari, 1994, 1995, 1996, Munari et al., 1997) also contain examples where the line appears in absorption, usually in systems with accretion disks in the bright state

Radial velocities of the Hα emission line (March data) were measured, using the cross correlation method. The same was done for the combined absorption and emission line of Hβ (February and March data). In view of the strong difference of the strength of the emission component during the two epochs the individual line profiles were cross-correlated not with the overall mean profile, but with the mean profile of the respective month. Alternatively, the emission component was masked and the cross-correlation was performed with the average profile of all data. Both approaches yielded consistent results. Hereafter, we will regard the radial velocities derived from the entire line profile.

The Hα radial velocities alone do not permit a reliable determination of a period because most of the March observations were performed in a single night and only one and two, respectively, spectra were taken in the two preceding nights. The Hβ data provide a longer time base, including the February observations. But even so their temporal distribution is far from ideal for a period analysis. The upper frame of Fig. 9 contains the Deeming (1975) power spectrum of all Hβ radial velocities. It contains a complicated alias pattern due to the extremely unequal data spacing. None of the peaks stands out to suggest itself as corresponding to the only reasonable radial velocity period. The four highest peaks suggest periods of $0^{\rm d}.192$, $0^{\rm d}.215$, $0^{\rm d}.234$, and $0^{\rm d}.270$, respectively. We will concentrate subsequently on the second of these values because using this choice results in an acceptable[5] (although still quite noisy) radial velocity curve not only for Hβ (shown in the second frame of Fig. 9 together with the best fit sine curve) when the data are folded on that period, but also for Hα (lower frame of the figure). Adopting any of the alternative periods results in even less convincing radial velocity curves. Using the best fit sine curves RV amplitudes were measured to be 34 ± 7 km/sec for Hα and 30 ± 5 km/sec for Hβ, respectively.

Thus, the radial velocity measurements suggest an orbital period of $P_{\rm orb} = 0^{\rm d}.21462 \pm 0^{\rm d}.00025$ ($\approx 5^{\rm h}9^{\rm m}$) which, however, we only regard as preliminary. Here, the error was estimated from the dispersion of a Gaussian fit to the power spectrum peak correponding to $P_{\rm orb}$. But note that the fine structure of the alias pattern caused by the separation of $\sim$40 days between the February and March observations permits other choices separated by 0.024 cycles/day from the orbital frequency corresponding to $P_{\rm orb}$. Moreover, we emphasize that – considering the alternative frequencies suggested by the power spectrum and the limited quality of the radial velocity measurements – the value of the orbital period chosen here still requires confirmation. However, it appears that the current observations are not compatible with the orbital period of $7^{\rm h}.59$ suggested by Patterson, marked by an arrow in the upper

[5] or should we say: the least unacceptable?

frame of Fig. 9.

4.2 Photometry

While no time resolved photometry of HQ Mon has ever been published the AAVSO data base contains light measurements performed with a cadence of $\sim 25^{\rm s}$ in three nights in 2003 March. These are reproduced in Fig. 10 in order to be compared with the new data of 2014 and 2015, presented in this paper (Fig. 11), binned to the same time resolution as the AAVSO data. To facilitate comparison the time and magnitude scales are the same in both figures.

HQ Mon exhibits night-to-night variations which can reach several tenths of a magnitude. This is compatible with the historical records and with the long-term AAVSO light curve (not shown) and is quite normal for cataclysmic variables. Superposed on these long-term light modulation is low-scale flickering with amplitudes of the order of $0\overset{\rm m}{.}03$ – $0\overset{\rm m}{.}04$[6], even smaller than observed in LS IV -08° 3 and the average UX UMa stars (see Sect. 3.2) but similar to the median flickering amplitude of $0\overset{\rm m}{.}035$ observed in the novalike variable IX Vel (calculated from the results of Beckemper 1995). Considering that HQ Mon does not exhibit dwarf nova outbursts and has also never been seen in the long-term AAVSO light curve to go into a low state it appears therefore most appropriate to classify the system as a *bona fide* UX UMa variable. This is in line with the spectral appearance i.e. hydrogen emission superposed on broad absorption lines and He II λ4686 in emission (Wahlgren et al. 1985).

The light curve of 2003, March 3 (upper frame of Fig. 10) exhibits an intriguing pattern of apparently regular oscillations with decreasing amplitude superposed on a gradual fading. To parameterize it, two sine curves were fit to the data (solid line in the figure), one with a long period ($\sim 54^{\rm h}$) accounting for the slow variations[7], and another with a short period following approximately the oscillations. The latter turns out to be about $41^{\rm m}$. Based on this light curve alone one might suspect an intermediate polar nature for HQ Mon, the $41^{\rm m}$ oscillation reflecting the rotation period of the white dwarf. However, since this pattern of variability does not repeat itself in other nights, this might well be an over interpretation of the data.

5 ST Cha

The classification history of ST Cha, discovered originally by Luyten (1934), was recently summarized by Simonsen et al. (2014). First considered to be an irregular variable or some kind of variable young star it entered the catalogues of CVs based on the suggestion of Cieslinski et al. (1998) who proposed a dwarf nova classification. This notion is founded on the spectrum of ST Cha which shows a strong blue continuum with broad and shallow absorptions in the higher Balmer lines and Hα in emission (but note that the blue and red parts of the spectrum were observed in different nights). Moreover, the $UBVRI$-colours of ST Cha, as measured by Cieslinski et al. (1997) are compatible with the colours normally encountered in CVs (Bruch & Engel, 1994; Echevarría, 1988).

The nature of ST Cha is discussed by Simonsenet al. (2014) based on the long-term AAVSO light curve. In particular its more recent parts have a dense coverage and therefore provide the most conclusive information. In Fig. 12 a 470 day section is shown, encompassing

[6] The larger scatter in the light curve of 2014, March 28 (top panel of Fig. 11), in particular near the end, is partly due to the extension of the observation to quite high air masses.

[7] This is only a parameterization! We neither claim that the slow variations are sinusoidal nor that they are periodic.

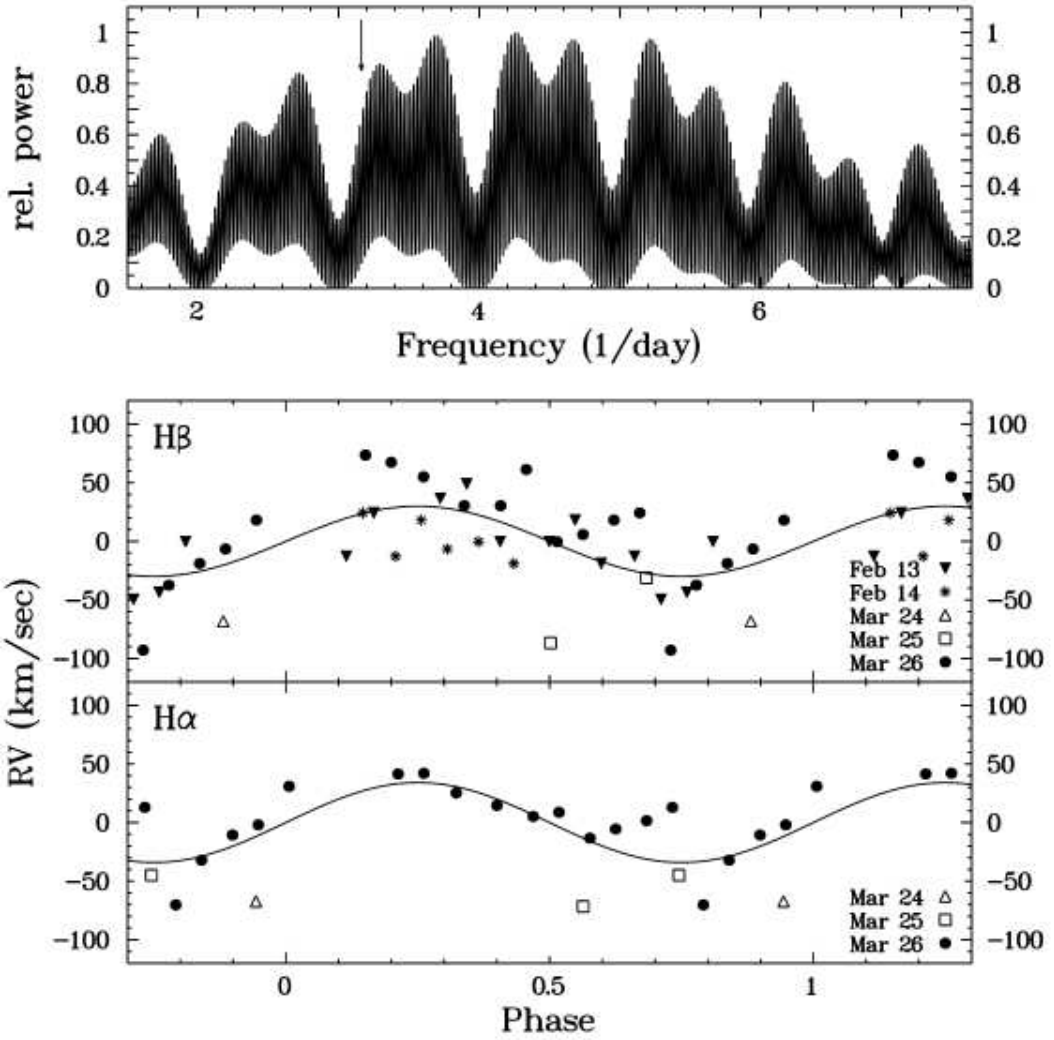

Figure 9: *Top:* Normalized power spectrum of the Hβ radial velocities of HQ Mon. The arrow indicates the frequency corresponding to the orbital period informally proposed by J. Patterson. *Bottom:* Radial velocities of Hβ (upper frame) and Hα (lower frame) folded on the period $P_{\rm orb} = 0^{\rm h}.21462$ suggested by the present data (see text).

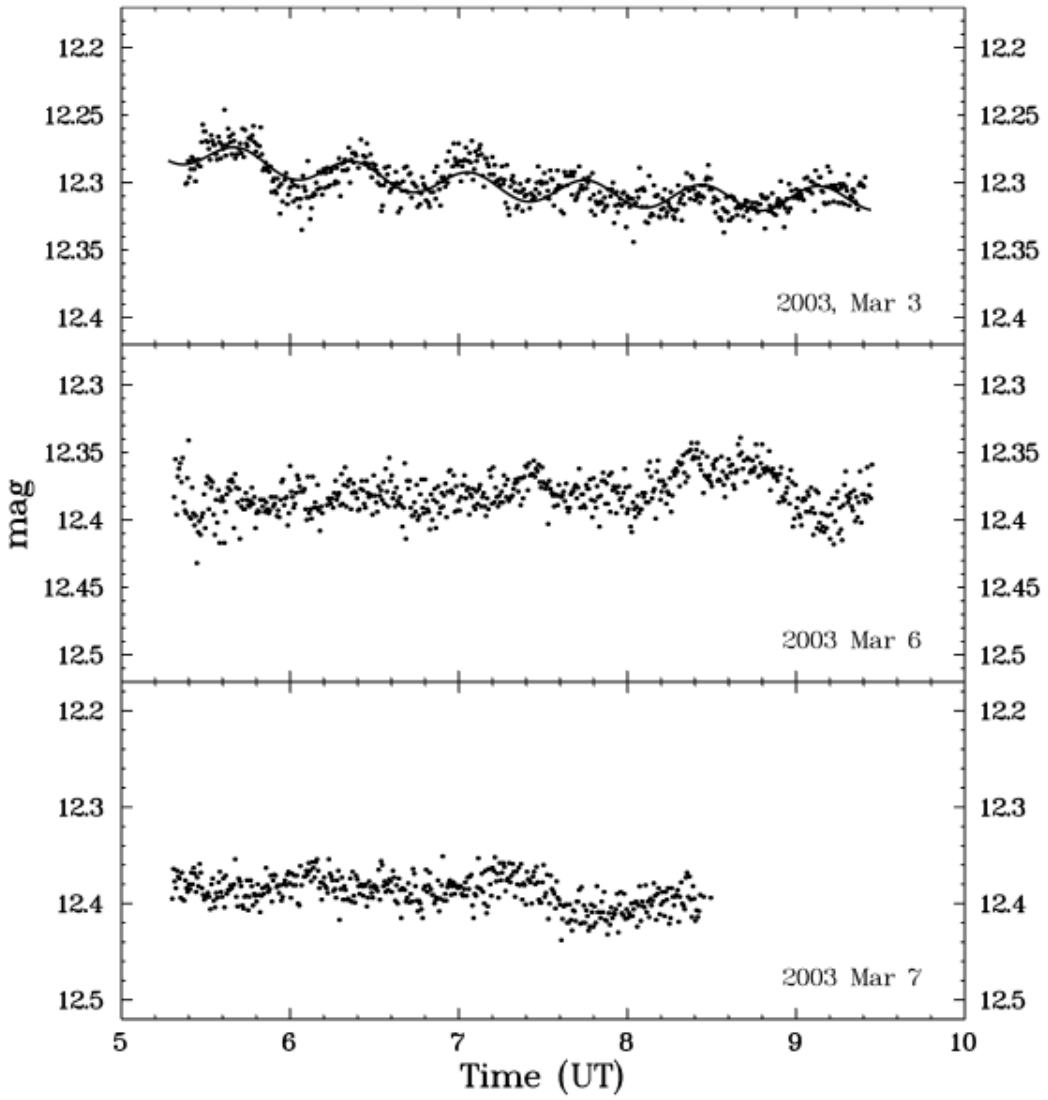

Figure 10: Light curves with $\sim 25^{s}$ time resolution from the AAVSO data base. The photometric band is not specified. The solid line in the upper frame represents a formal two component sine fit to the data (see text for details).

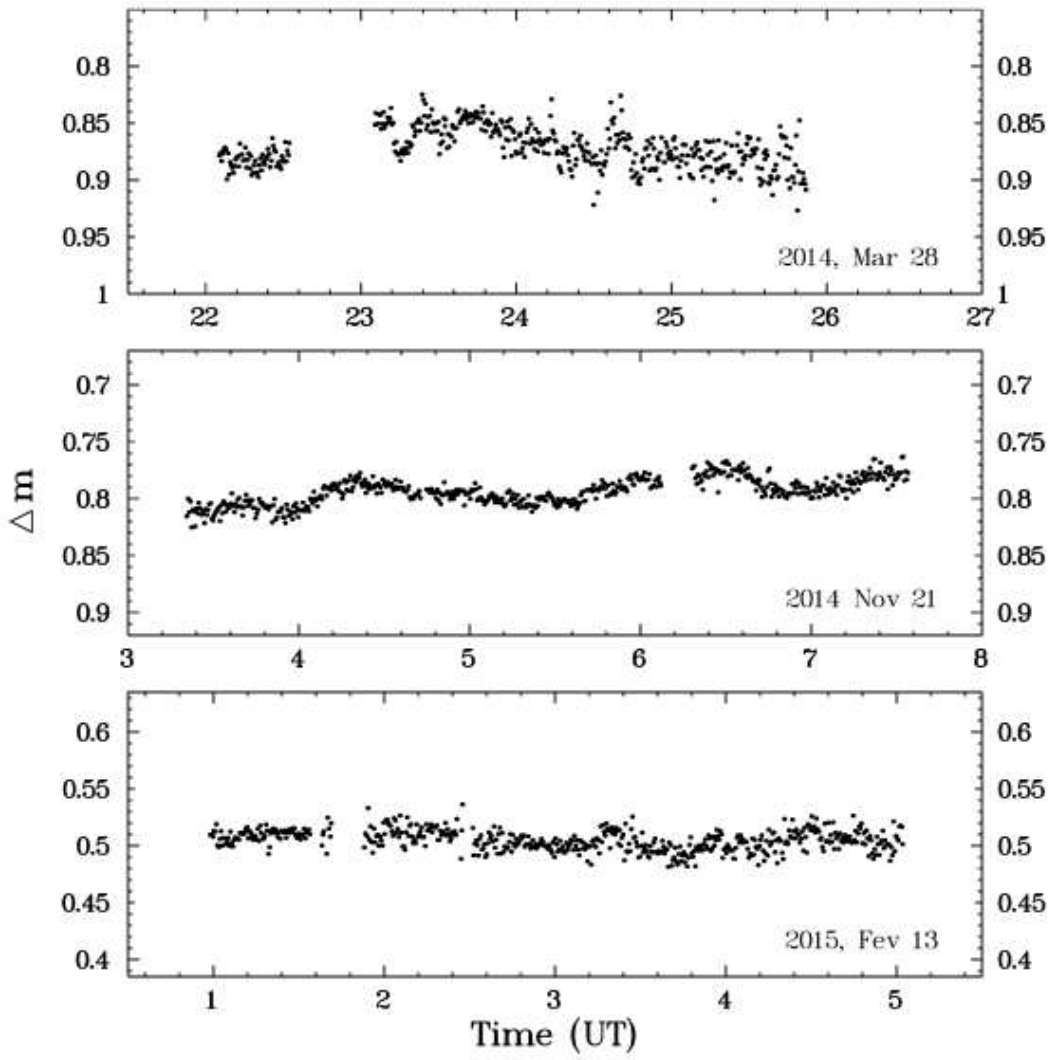

Figure 11: Time resolved differential light curve of HQ Mon in three nights in 2014 and 2015.

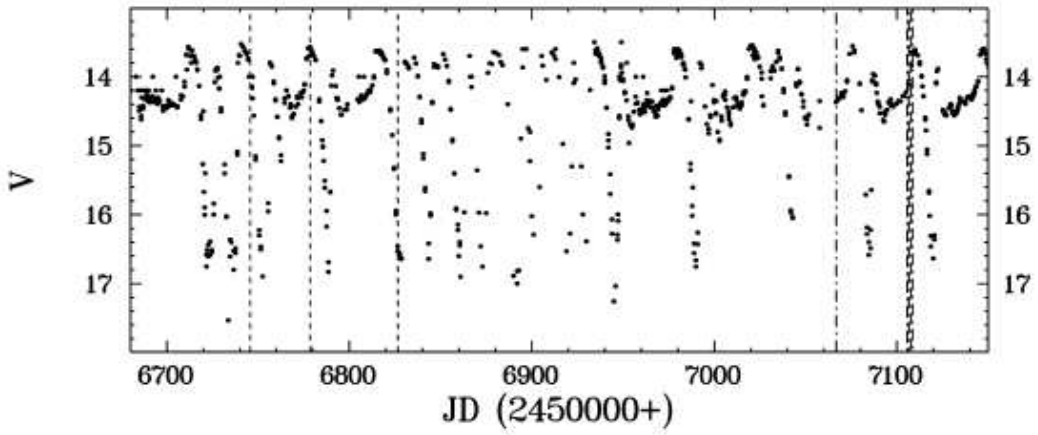

Figure 12: Part of the AAVSO long-term light curve of of ST Cha. The epochs of the present photometric and spectroscopic observations are indicated by vertical dashed and dashed-dotted lines, respectively.

the dates of the presently discussed photometric and spectroscopic observations which are indicated by the vertical dashed and dashed-dotted lines, respectively. Most of the data points are CCD V magnitudes with some visual magnitudes interspersed. The light curve reveals outbursts in rapid succession with only quite short excursions to a faint (minimum) state, sometimes interrupted by standstills at a level slightly below maximum magnitude. This behaviour is the hallmark of Z Cam stars, and consequently Simonsen et al. (2014) classify ST Cha as such.

Cieslinski et al. (1998) mention that ST Cha possibly exhibits eclipses with a period of 6.8 hours (0.283 days) or 9.6 hours (0.4 days). This is based on a light curve published in tabular form by Mauder & Sosna (1975), measured on 91 photographic plates distributed (inhomogeneously) over a time interval of 124 days in 1971-72. To have a closer look at this issue, we reproduce a graph of their light curve in Fig. 13 (upper frame). The mean photometric magnitude is $\sim 14^{\rm m}.25$, and the total range of variability spans about $1^{\rm m}$.

Various period search tools were applied to the light curve: phase dispersion minimization (Stellingwerf 1978), analysis of variance (AoV; Schwarzenberg-Czerny 1989), and power spectrum analysis following Lomb (1976) and Scargle (1982). While the latter is expected to be more sensitive to sinusoidal variations the other two methods depend less strongly on the waveform of a supposed periodic signal, but all of them yield compatible results.

The Lomb-Scargle periodogram is shown in central frame of Fig. 13. It reveils a strong alias pattern with the highest peak at a frequency of 3.505/day. This corresponds to a period of 0.2853 days or 6.847 hours, equal to one of the periods suggested by Cieslinski et al. (1998). Their alternative period corresponds to the frequency of the next strong alias peak at lower frequencies in the power spectrum.

Folding the data on the various periods it is difficult to decide which of the aliases is to be preferred. The lower frame of Fig. 13 shows the folded light curve, using a period of 0.28535 days[8] (henceforth referred to as $P_{\rm MS}$). Considering the likely errors of photographic photometry the resulting curve is satisfactory, but is is hardly the light curve of an eclipsing

[8]No effort has been made to align the minimum in the folded light curve to phase zero which is simply defined by the observing time of the first data point in the light curve. Thus, the minimum coinciding with phase zero is merely fortuitous.

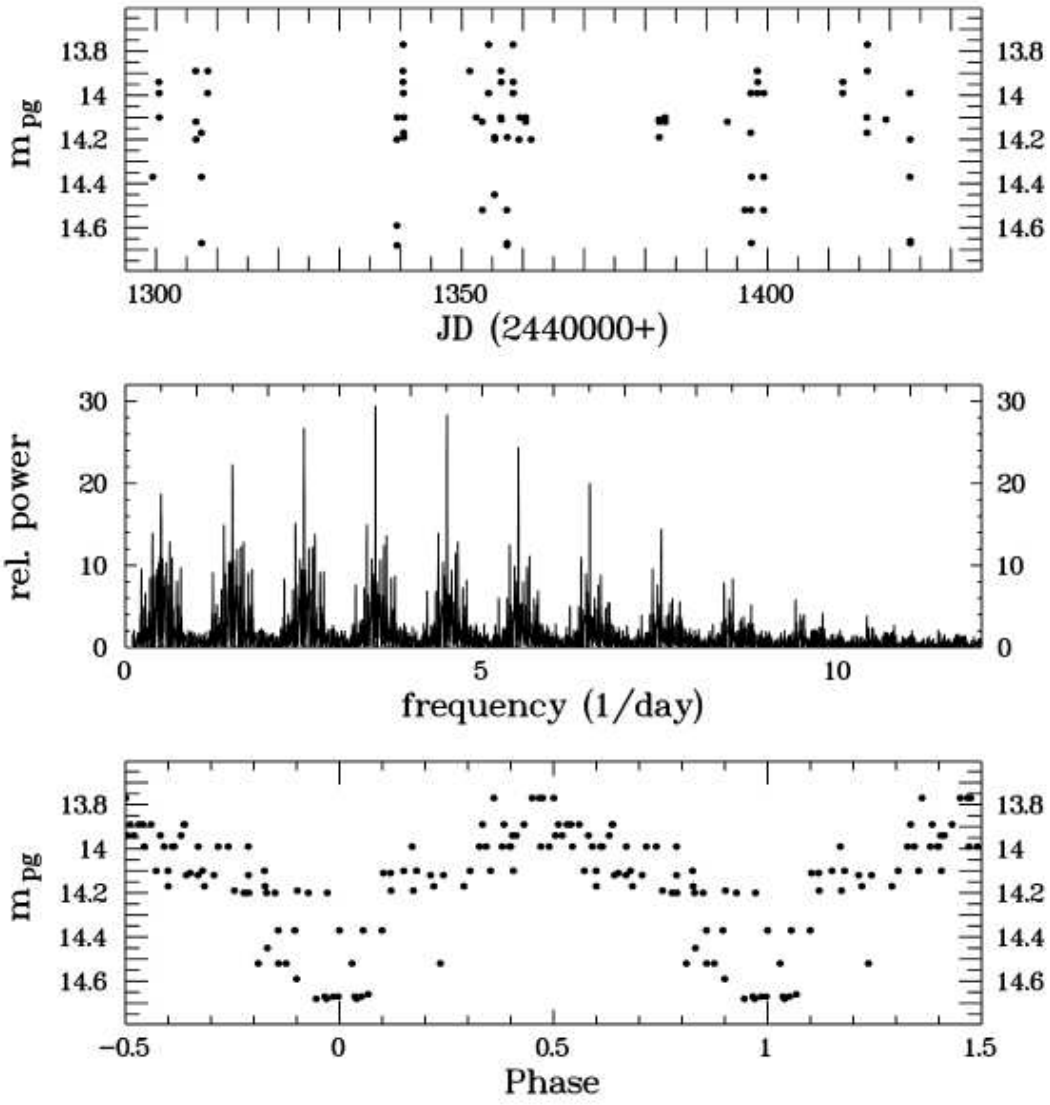

Figure 13: *Upper frame:* Long-term photographic light curve of ST Cha observed by Mauder & Sosna (1975). *Middle frame:* Lomb-Scargle periodogram of the light curve. *Lower frame:* The light curve folded on the period 0.28535 days).

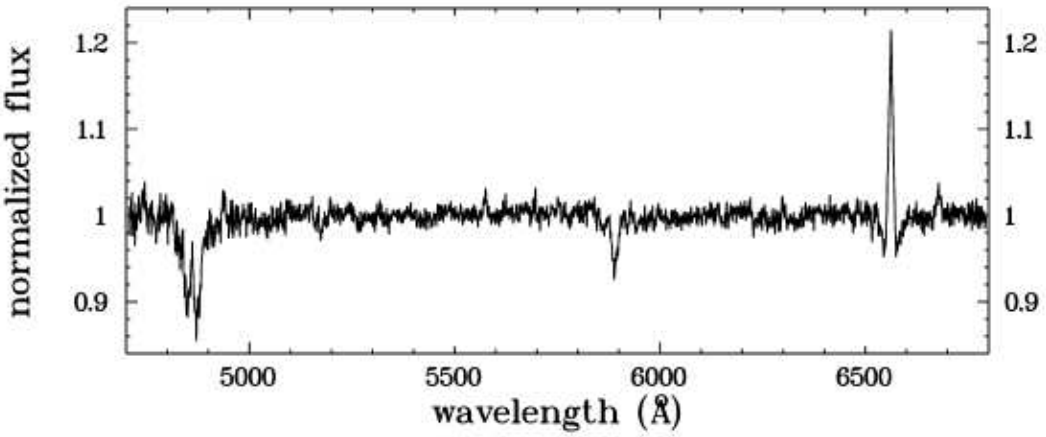

Figure 14: Average continuum-normalized spectrum of ST Cha

cataclysmic variable.

As a caveat it must be mentioned that the alias frequencies in the periodograms can all be explained as harmonics of one fundamental frequencies which corresponds exactly (within the resolution) to a period of 2 solar days. While it is not obvious what observational effect could cause a spurious period with that value the very close coincidence of the fundamental period with a multiple of one day may raise some concern as to the reality of the observed period.

5.1 Spectroscopy

Spectra of ST Cha were obtained in one night in 2015, February and in four subsequent nights in 2015, March (see Table 2). The AAVSO light curve (Fig. 12) shows that the February observations were taken during a standstill, while in March ST Cha was on the final rise from a standstill to an outburst. The February data are extremely noisy and will therefore not be regarded. During the four nights in March no significant changes of the spectrum were observed. Therefore, the average spectrum, weighing the individual spectra by their mean count rates, was calculated and is shown in Fig. 14.

The spectrum is dominated by a strong Hα emission line located within a shallow broad absorption component. Hβ as a much fainter emission component, while the absorption is significantly stronger than in Hα. This behaviour is as expected for a dwarf nova in outburst or standstill. The only other positively identified stellar line is a faint emission of He I at λ 6678 Å. Another similarly strong structure close to λ 5577 Å is evidently caused by the telluric [O I] auroral line not perfectly removed by the spectral extraction procedure. ST Cha being close to the maximum of an outburst makes it unlikely that absorption features of the secondary star should be present in the spectrum. This, together with the absence of any other late type absorption feature suggests that the strong Na D absorption lines seen just short ward of λ 5900 Å has an interstellar origin.

In order to measure the orbital period of ST Cha, an attempt was made to determine the radial velocity variations of the Hα emission line, using the cross correlation technique mentioned earlier. Only the data of 2015, March 24 and 25 were considered because of the larger number of exposures in these nights and their – on average – better signal-to-noise ratio as compared to the spectra taken during the other nights. Even so, some individual

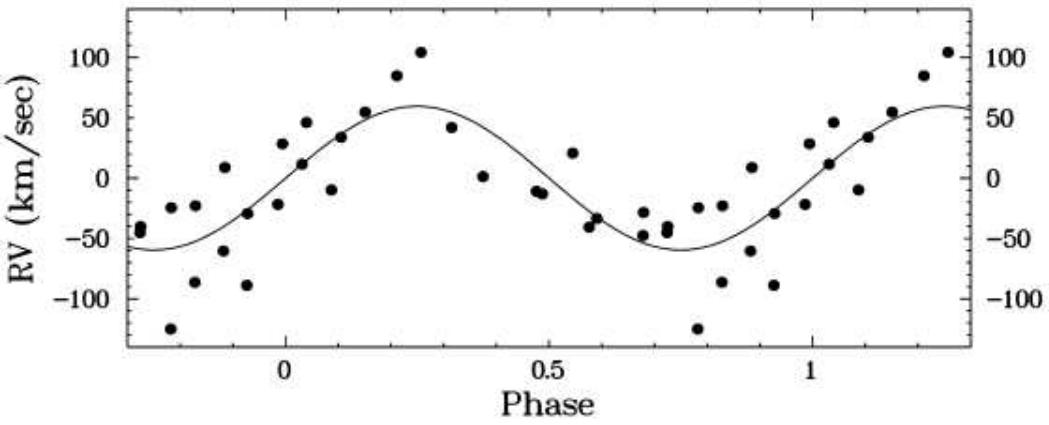

Figure 15: Radial velocities of Hα (dots) of ST Cha observed on 2015, March 24 and 25, folded on the period $P = 0.229$ days together with the best fit sine curve (solid line).

spectra were rejected because their Hα line did not stand out sufficiently well from the noise in the surrounding region.

The results were subjected to several period search routines. The AoV method, the Lomb-Scargle periodogram, the Deeming (1975) power spectrum and a least squares sine fit all pointed at the same period within a small range of 0.006 days. The average value is $P_{\rm orb} = 0.229$ days which we will regard as the orbital period of ST Cha. The data folded on $P_{\rm orb}$ are shown together with the best fit sine curve in Fig. 15. We cannot exclude the possibility that the true period is a 1/day alias of this value. However, folding the data on any one of these yields a less convincing RV curve. The radial velocity amplitude is 60 $\pm$ 9 km/sec. The velocity zero point (γ-velocity) is evidently determined by the peak of the average Hα line and has no physical meaning. Therefore, γ has been subtracted from the curve in the figure.

An error derived from the scatter of the period determined using the different methods quoted above is unrealistically small because the methods are not independent from each other. A more realistic period error may be determined from the width of the peak corresponding to the orbital frequency in the power spectra. The width (standard deviation) of a Gaussian fit to this peak in the Deeming (1975) power spectrum corresponds to $\pm 0^{\rm d}.015$.

5.2 Photometry

We obtained time resolved differential photometry of ST Cha in three nights in 2014. UCAC4 053-009413, taken from the Forth USNO CCD Astrograph Catalogue (Zacharias et al. 2013) served as a comparison star. Its magnitude is quoted by Zacharias et al. (2013) as $V = 12^{\rm m}.317$. The present light curves have an average differential magitude Δm of $1^{\rm m}.82$ on March 29, $1^{\rm m}.52$ on April 30 and $4^{\rm m}.08$ on June 17. Assuming that the effective wavelength of the current white light observations corresponds roughly to V the approximate visual magnitude of ST Cha during the three observing nights was thus $14^{\rm m}.1$, $13^{\rm m}.8$ and $16^{\rm m}.4$, respectively. This is consistent with the magnitude of ST Cha at the observing dates in the long term light curve shown in Fig. 12.

During the observations in March and April, shown in the upper two frames of Fig. 16, in particular on March 29, the observing conditions were far from ideal. Thus, the individual data points, observed with a time resolution of $\sim 5^{\rm s}$ show a large scatter. Therefore, for the

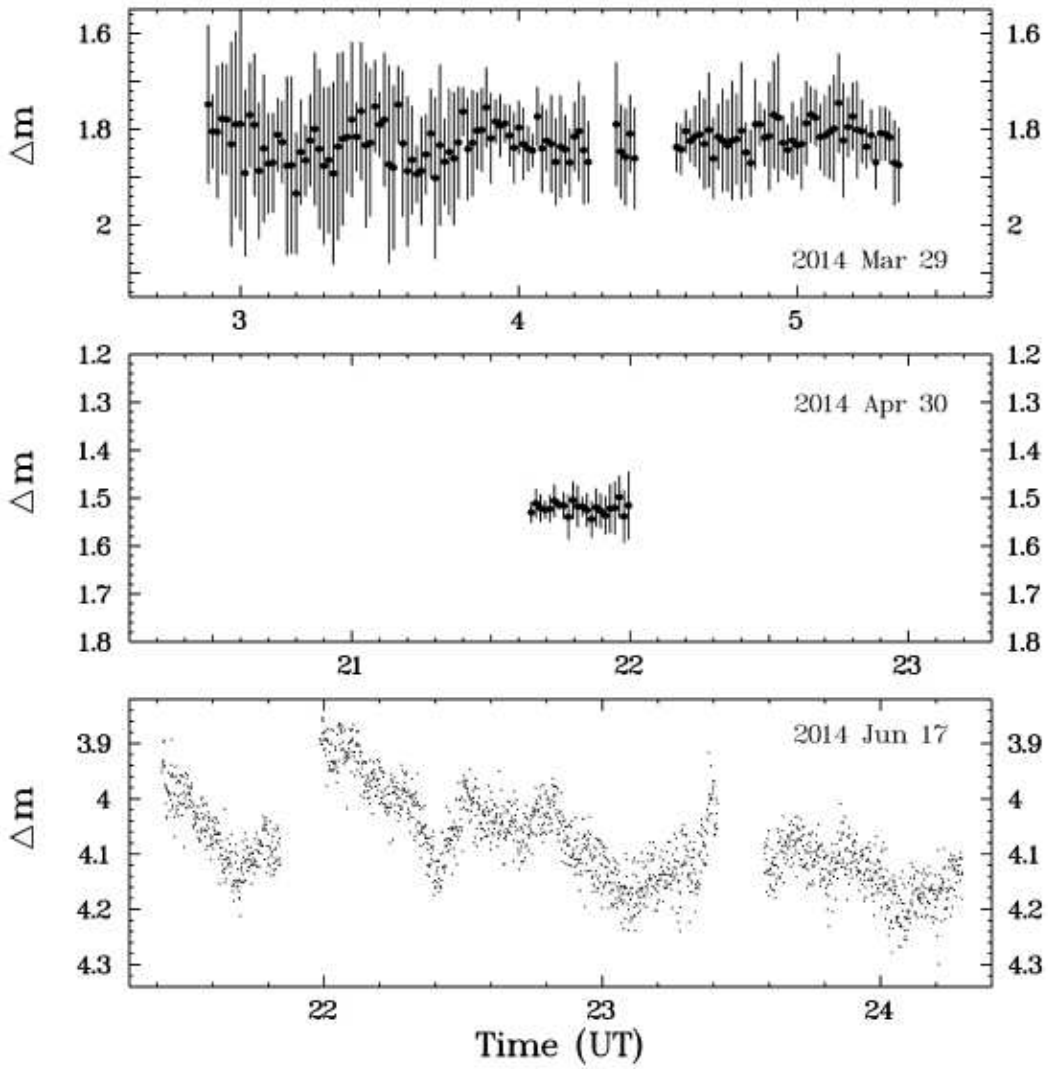

Figure 16: Differential light curves of ST Cha in three nights. In the upper two frames the original time resolution was degraded by binning the data into 1^{m} intervals. The vertical lines indicate the standard deviation of the original data points around the bin average.

purpose of visualization the data points were binned in intervals of $1^{\rm m}$ and the error bars shown in the figure represent the standard deviation of the individual data points within each bin.

On March 29, ST Cha was starting a rapid decline from an outburst. Because of the unfavourable weather conditions the time resolved light curve is quite noisy even after data binning. The scatter of the binned data points remains within the limits defined by the errors. Therefore, it is not immediately clear if the observed variations are real – due to flickering – or if they are just caused by noise. An analysis of the correlation between neighbouring data points, employing R statistics, may help. This method, first introduced by Baptista & Steiner (1993) and later refined by Bruch (1999), basically determines whether neighbouring points in an ensemble of data scattered around zero have preferentially the same sign or whether the sign changes statistically (as they should for a random data set with zero mean). Applying R statistics to the residuals between the binned data points of 2015, March 29 and a straight line fitted by least squares to these data, yields a probability of 0.9992 for correlations between the data points. It may thus be concluded that the variations seen in the light curves are not just accidental but that at least a part of them are real.

The light curve of April 30 is much shorter. It was observed right at the maximum of an outburst following a standstill of ST Cha. During this night the scatter of the individual data points is significantly smaller[9]. Again, R statistics were applied to see if the residual scatter shows correlations or not. The probability that the data within the observed $\sim 22^{\rm m}$ interval are indeed correlated is low: 0.10. Thus, any flickering which might have been present remained below the detection threshold.

The light curve of June 17 was obtained under much better atmospheric conditions, but also in an different photometric state. As can be seen in Fig. 12, ST Cha was close to the bottom of a short minimum between two outbursts. Considering the size of the telescope and the short exposure times the faint magnitude explains the considerable noise in the light curve. Even so considerable flickering activity is evident.

5.3 The photometric period

Having presented spectroscopic observation, the AAVSO light curve and additional time resolved photometry it is time to return to the question of the period $P_{\rm MS}$ derived from the observations of Mauder & Sosna (1975).

There are many reasons to suspect that there is something wrong with those data. The foremost argument may be the contradiction with the spectroscopic orbital period of ST Cha. On the other hand, $P_{\rm MS}$ is based on photometric variations which may not reflect the orbital motion but some other variability of the system. If so, it must have been transient because it does not show up in more recent AAVSO data or in the present photometry.

Allowing for some observational scatter the total amplitude of the variations seen in the lower frame of Fig. 13 is of the order of $0\overset{\rm m}{.}8$. The time between minimum and maximum is about $3\overset{\rm h}{.}4$. The mean photographic magnitude of $12\overset{\rm m}{.}2$ corresponds approximately to the average white light magnitude observed on March 29. Since that light curve has a duration of about $2\overset{\rm h}{.}5$ any variation of the type found in the data of Mauder & Sosna (1975) should have left a clear trace in the light curve, even considering the adverse atmospheric conditions. The same is true for the even longer light curve of June 17 which, however, was taken during a much fainter state. The AAVSO light curve does not encompass the epoch of the Mauder & Sosna (1975) observations. It may not have the time resolution to show periodicities of the order of hours. However, if variations similar to those seen in Fig. 13 would have been

[9]Note that the magnitude scale in all panels of Fig. 16 is the same.

present during the longer standstills of ST Cha (see Fig. 12), they should have caused a considerably stronger scatter in magnitude than actually observed.

The origin of the strong variations and the periodicity in the data of Mauder & Sosna (1975) therefore remains unclear. Having no convincing explanation we leave the question open.

6 Conclusions

With the intention to better characterize these system, we have presented spectroscopic and photometric data of three bright cataclysmic variables. Only for LS IV -08^{o} 3 a reliably determined orbital period had already been published in the literature by Stark et al. (2008). The present data confirm many of their findings, permitted to improve the ephemeris of the system, and provided some additional information. For the other two systems, HQ Mon and ST Cha, we publish for the first time time-resolved spectroscopy and high time resolution photometry[10]. We find that previous unconfirmed values for the orbital period of these systems, circulating in the literature, are erroneous and derived alternative values from radial velocity measurements. However, in particular for HQ Mon the proposed orbital period still requires independent confirmation.

Acknowledgements

We gratefully acknowledge the use of the AAVSO data base which provided valuable supportive information for this study.

References

Baptista, R., & Steiner, J.E. 1993, A&A 277, 311

Beckemper, S. 1995, Statistische Untersuchungen zur Stärke des Flickering in kataklysmischen Veränderlichen, Diploma thesis, Münster

Bruch, A. 1982, PASP, 94, 562

Bruch, A. 1989, A&AS, 78, 145

Bruch, A. 1993, MIRA: A Reference Guide (Astron. Inst. Univ. Münster

Bruch, A. 1999, AJ, 117, 3031

Bruch, A. 2016, New Astr., 46, 60

Bruch, A., & Engel, A. 1994, A&AS, 104, 79

Bruch, A., & Schimpke, T. 1992, A&AS, 93, 419

Cieslinski, D., Jablonski, F.J., & Steiner, J.E. 1997, A&AS 124, 55

Cieslinski, D., Steiner, J.E., & Jablonski, F.J. 1998, A&AS 131, 119

Deeming, T.J. 1975, Ap&SS, 39, 447

[10]noting that to our knowledge the high time resolution light curves of ST Cha found on the AAVSO website have not otherwise been published.

Diaz, M. & Hubeny, I. 1999, ApJ, 523, 786

Eastman, J., Siverd, R., & Gaudi, B.S. 2010, PASP, 122, 935

Echevarría, J. 1988, Rex. Mex. A&A, 16, 37

Hellier, C. 2001, Cataclysmic Variable Stars, Springer Verlag, Berlin

Høg, E., Fabricius, C., Makarov, V.V., et al. 2000, A&A, 355, L27

Knigge, C. 2011, MNRAS, 373, 484

Knigge, C., Baraffe, I., & Patterson, J. 2011, ApJ Suppl., 194, 28

Lomb, N.R. 1976, ApSS, 39, 447

Lloyd Evans, T. 1984, The Observatory, 104, 221

Luyten, W.J. 1934, AN 253, 135

Mauder, H., Sosna F.M. 1975, IBVS 1049

Morgenroth, O. 1933, Astron. Nachr. 249, 385

Munari, U., Zwitter, T., & Bragaglia, A. 1997, A&AS, 122,495

Nassau, J.J., Stephenson, C.B. 1963, Hamburger Sternw., Warner & Swasey Obs.

Ritter, H., Kolb, U. 2003, A&A, 404, 301

Rosenfeld, A., Kak, C.A. 1982, Digital Picture Processing, Academic Press, New York, p. 353

Samus, N.N., Durlevich, O.V., Kazarovetz, E.V., et al. 1975, General Catalogue of Variable Stars, http://www.sai.msu.su/gcvs/gcvs/

Scargle, J.D. 1982, ApJ, 263, 853

Schmidt-Kaler, Th. 1982, in: K. Schaifers, H.H. Voigt (eds.): Landolt Börnstein, Numerical Data and Functional Relationships in Science and Technology, New Series, Group VI, Vol. 2, Subvol. b, Springer Verlag, Heidelberg, p. 1

Schneider, D.P., & Young, P. 1980, ApJ, 238, 946

Schreiber, M.R., Zorotovic, M., & Wijnen, T.P.G. 2016 MNRAS, 455, L16

Schwarzenberg-Czerny, A. 1989, MNRAS, 241, 153

Shafter, A.W. 1983, ApJ, 267, 222

Shafter, A.W., Szkody, P., & Thorstensen, J.R. 1986, ApJ, 308, 765

Simonsen,M., Bohlsen, T., Hambsch, F.-J., & Stubbings, R. 2014, JAAVSO, 42

Stark, M.A., Wade, R.A., Thorstenson, J.R., et al. 2008, AJ, 135, 991

Stellingwerf, R.F. 1978, ApJ, 224, 953

van Bueren, H.G. 1950, Ann. Sterrew. Leiden,20, 201

Wahlgren, G.M. 1992, AJ, 104, 1174

Wahlgren, G.M., Wing, R.F., Kaitchuck, R.H., et al. 1985, BAAS 17, 599

Warner, B. 1995, Cataclysmic Variable Stars, Cambridge Astrophysics Series, Cambridge Univ. Press

Zacharias, N., Finch, C.T., Girard, T.M., et aql. 2013, AJ, 145, 44

Zorotovic, M., Schreiber, M.R. & Gänsicke, B.T. 2011, A&A, 536, A42

Zwitter, T., & Munari, U. 1994, A&AS, 107, 503

Zwitter, T., & Munari, U. 1995, A&AS, 115, 575

Zwitter, T., & Munari, U. 1996, A&AS, 117, 44